Progress In Electromagnetics Research B, Vol. 35, 187–212, 2011

LOW-FREQUENCY SCATTERING ANALYSIS AND HOMOGENISATION OF SPLIT-RING ELEMENTS

J. C.-E. Sten[1] and D. Sjöberg[2,*]

[1]Technical Research Centre of Finland, 02044 VTT, Finland

[2]Department of Electrical and Information Technology, Lund University, P. O. Box 118, 221 00 Lund, Sweden

Abstract—A key structure in so-called metamaterial mediums is the elementary split-ring resonator. We consider in this paper the low-frequency electromagnetic scattering by a split-ring particle modelled as a perfectly conducting wire ring, furnished with a narrow gap, and derive analytical solutions for the electric and magnetic dipole moments for different kinds of incidence and polarisation in the quasi-static approximation. Through a vectorial homogenisation process, the expressions discovered for the dipole moments and the related polarisability dyadics are linked with the macroscopic constitutive equations for the medium. We further show that the condition for resonance of a medium consisting of simple split-rings cannot be achieved by means of the given quasi-static terms without violating the underlying assumptions of homogenisation. Nevertheless, the results are applicable for sparse medium of rings, and we derive numerical guidelines for the applicability with some examples of the effect of the considered split-ring medium on electromagnetic wave propagation.

1. INTRODUCTION

The split-ring resonator, or a ring shaped metal particle with a gap, has been identified as a crucial ingredient of so-called "metamaterial" mediums, known to display the extraordinary electromagnetic property of negative refraction and negative permeability and permittivity [1]. To analyse the response of such a particle or an assembly of such particles to an impinging electromagnetic wave, different semi-heuristic models involving the concepts of capacitance and inductance

Received 6 September 2011, Accepted 13 October 2011, Scheduled 28 October 2011

* Corresponding author: Daniel Sjöberg (daniel.sjoberg@eit.lth.se).

have previously been adopted [1, 2]. Such models may often be adjusted to perform satisfactorily, but for the sake of gaining physical understanding, a model where the polarisation is seen to arise from the dipole moments of the individual constituent particles would be more insightful.

In this paper, we present a low-frequency scattering analysis for discovering the quasi-static multipole moments of a split-ring element for different types of incidence and an application of the derived dipole moments to medium homogenisation. Other approaches to this problem are scarce, e.g., [3, 4], but there are some analytical results for two-dimensional versions of the geometry [5, 6]. We note that high-ϵ dielectric resonators [7] may provide an efficient alternative to split-ring resonators as constituent "molecules" of a medium displaying extraordinary magnetic properties.

We begin with the formulation and the solution of the relevant problems of low-frequency electromagnetic scattering by an isolated split-ring element. The analysis of the pertinent polarisation, charges and currents induced on the ring is carried out approximately by assuming the wire to be thin and the gap to be narrow in comparison to the diameter of the split-ring. Moreover, every dimension is required to be much smaller than the wavelength in the medium, to ensure that the quasi-static assumptions apply. The formulation and solution of the pertaining integral equations, although carried out by means of approximations in terms of elementary and trigonometric functions, is rather involved especially due to the presence of the gap, which brings about a break in the otherwise symmetric particle.

Next, using the multipole moments, dipole moments or the elements of the polarisability dyadics are formed that characterise the scattering properties of the constituent particles at low frequencies [8–11]. As a bonus, the analysis yields the quadrupole moments, which offer the first order correction to the dipolar field. At low frequencies these terms are significant only at distances very close to the particles, and they are left out of account when the homogenisation by means of Lorentz-Lorenz-approach is performed. In the homogenisation, we assume the medium to consist of equally oriented split-rings, but the same analysis can be performed with any other ordered assembly of rings. The benefit of our formulation is that the dependence of the material parameters on the geometry of the rings (wire thickness, ring radius, gap width and mutual distance), the frequency and polarisation, is given explicitly, thus providing useful insight into the workings of the medium. The result is a 6×6 matrix with ten nonzero entries, characteristic of a bi-anisotropic medium. We point out that the quasi-static dipole moments alone do not correctly predict the

singularity of the medium, at which the medium parameters experience a resonance type of behavior, because of a packing density which violates the conditions for homogenisation. Finally, we discuss possible engineering applications and limitations of the split-ring medium in view of the homogenisation result and, in particular, derive a direct link between the refractive indices and the geometrical parameters of a birefringent split-ring medium.

2. FORMULATION OF THE SCATTERING PROBLEM

2.1. Integral Equations

As a general introduction we first formulate the problem of electromagnetic scattering by an inhomogeneity occupying the volume V, having the permittivity ϵ and the permeability μ, the values outside V being ϵ_0 and μ_0. Assuming $e^{j\omega t}$-harmonicity of the fields in time, the Maxwell equations read [8]

$$\nabla \times \mathbf{E} + j\omega\mu_0\mathbf{H} = -j\omega(\mu - \mu_0)\mathbf{H} \equiv -\mathbf{J}_m, \tag{1}$$

$$\nabla \times \mathbf{H} - j\omega\epsilon_0\mathbf{E} = j\omega(\epsilon - \epsilon_0)\mathbf{E} \equiv \mathbf{J}_e, \tag{2}$$

with $\nabla \cdot (\epsilon\mathbf{E}) = 0$ and $\nabla \cdot (\mu\mathbf{H}) = 0$. Equations (1) and (2) define the equivalent magnetisation current density $\mathbf{J}_m$ and the equivalent electric polarisation current density $\mathbf{J}_e$, respectively, which satisfy the respective equation of continuity $\nabla \cdot \mathbf{J}_m = -j\omega\varrho_m$ and $\nabla \cdot \mathbf{J}_e = -j\omega\varrho_e$, where ϱ_e, ϱ_m are the electric and magnetic charges set into oscillation.

When an electromagnetic field $\mathbf{E}^{inc}$, $\mathbf{H}^{inc}$ impinges on the obstacle, the field is governed by the pair of volume integral equations [8]:

$$\begin{aligned}\mathbf{E}(\mathbf{r}) &= \mathbf{E}^{inc}(\mathbf{r}) + \left(\mathbf{I}k^2 + \nabla\nabla\right) \cdot \int_V \frac{e^{-jk|\mathbf{r}-\mathbf{r}'|}}{4\pi|\mathbf{r}-\mathbf{r}'|} \frac{\mathbf{J}_e(\mathbf{r}')}{j\omega\epsilon_0} dV(\mathbf{r}') \\ &\quad -\nabla \times \int_V \frac{e^{-jk|\mathbf{r}-\mathbf{r}'|}}{4\pi|\mathbf{r}-\mathbf{r}'|} \mathbf{J}_m(\mathbf{r}')dV(\mathbf{r}'),\end{aligned} \tag{3}$$

$$\begin{aligned}\mathbf{H}(\mathbf{r}) &= \mathbf{H}^{inc}(\mathbf{r}) + \left(\mathbf{I}k^2 + \nabla\nabla\right) \cdot \int_V \frac{e^{-jk|\mathbf{r}-\mathbf{r}'|}}{4\pi|\mathbf{r}-\mathbf{r}'|} \frac{\mathbf{J}_m(\mathbf{r}')}{j\omega\mu_0} dV(\mathbf{r}') \\ &\quad +\nabla \times \int_V \frac{e^{-jk|\mathbf{r}-\mathbf{r}'|}}{4\pi|\mathbf{r}-\mathbf{r}'|} \mathbf{J}_e(\mathbf{r}')dV(\mathbf{r}'),\end{aligned} \tag{4}$$

where $k = \omega\sqrt{\mu_0\epsilon_0}$ is the wave number, $\omega/2\pi$ is the oscillation frequency and $\mathbf{I}$ the unit dyadic. At a large distance from the scatterer,

where $r = |\mathbf{r}| \gg |\mathbf{r}'|$, we may approximate $e^{-jk|\mathbf{r}-\mathbf{r}'|}/|\mathbf{r}-\mathbf{r}'| \approx e^{-jkr+jk\hat{\mathbf{r}}\cdot\mathbf{r}'}/r$. Then, the scattered field is

$$\mathbf{E}(\mathbf{r}) - \mathbf{E}^{inc}(\mathbf{r}) \approx -\frac{jk^2}{\omega\epsilon_0}\frac{e^{-jkr}}{4\pi r}(\mathbf{I}-\hat{\mathbf{r}}\hat{\mathbf{r}})\cdot\int_V e^{jk\hat{\mathbf{r}}\cdot\mathbf{r}'}\mathbf{J}_e(\mathbf{r}')dV(\mathbf{r}') + jk\frac{e^{-jkr}}{4\pi r}\hat{\mathbf{r}}\times\int_V e^{jk\hat{\mathbf{r}}\cdot\mathbf{r}'}\mathbf{J}_m(\mathbf{r}')dV(\mathbf{r}'), \quad (5)$$

$$\mathbf{H}(\mathbf{r}) - \mathbf{H}^{inc}(\mathbf{r}) \approx -\frac{jk^2}{\omega\mu_0}\frac{e^{-jkr}}{4\pi r}(\mathbf{I}-\hat{\mathbf{r}}\hat{\mathbf{r}})\cdot\int_V e^{jk\hat{\mathbf{r}}\cdot\mathbf{r}'}\mathbf{J}_m(\mathbf{r}')dV(\mathbf{r}') - jk\frac{e^{-jkr}}{4\pi r}\hat{\mathbf{r}}\times\int_V e^{jk\hat{\mathbf{r}}\cdot\mathbf{r}'}\mathbf{J}_e(\mathbf{r}')dV(\mathbf{r}'). \quad (6)$$

If the scatterer is impenetrable for the electromagnetic field, as for a perfect conductor considered next, we note that the same formulation prevails, but $\mathbf{J}_e$ and $\mathbf{J}_m$ must then be interpreted as surface current densities with the volume integrals being duly replaced by integrals over a surface element dS'.

2.2. Low Frequency Multipole Expansion

When the frequency of oscillation is low enough, so that the characteristic dimension of the scatterer is much smaller than the wavelength in the medium, the field quantities may be written as a Rayleigh-Stevenson series expansion in terms of frequency [9, 10]. In particular, by Taylor-expanding the exponential $e^{-jk|\mathbf{r}-\mathbf{r}'|} = 1 - jk|\mathbf{r}-\mathbf{r}'| - \ldots$, the integral Equations (3)–(4) fall into different order in ω. The quasi-static equations are

$$\mathbf{E}_0(\mathbf{r}) = \mathbf{E}_0^{inc}(\mathbf{r}) + \nabla\nabla\cdot\int_V \frac{1}{4\pi|\mathbf{r}-\mathbf{r}'|}\frac{\mathbf{J}_{e,1}(\mathbf{r}')}{j\omega\epsilon_0}dV(\mathbf{r}'), \quad (7)$$

$$\mathbf{H}_0(\mathbf{r}) = \mathbf{H}_0^{inc}(\mathbf{r}) + \nabla\nabla\cdot\int_V \frac{1}{4\pi|\mathbf{r}-\mathbf{r}'|}\frac{\mathbf{J}_{m,1}(\mathbf{r}')}{j\omega\mu_0}dV(\mathbf{r}'), \quad (8)$$

the following being the first-order equations [10], and so on. The lowest order fields, $\mathbf{E}_0$ and $\mathbf{H}_0$, can be solved independently from (7) and (8), respectively, while the subsequent field terms $\mathbf{E}_1$, $\mathbf{H}_1$ etc. depend on those of previous order.

When the electromagnetic problem has been solved, the scattered far-field is found by evaluating (5) and (6). On account of the low frequency argument, $e^{jk\hat{\mathbf{r}}\cdot\mathbf{r}'} \approx 1 + jk\hat{\mathbf{r}}\cdot\mathbf{r}'$, Equations (5) and (6) can be

expressed

$$\mathbf{E}(\mathbf{r}) - \mathbf{E}^{inc}(\mathbf{r}) \approx k^2 \frac{e^{-jkr}}{4\pi\epsilon_0 r}\left[(\mathbf{I} - \hat{\mathbf{r}}\hat{\mathbf{r}}) \cdot \left(\mathbf{p}_e + jk\frac{\hat{\mathbf{r}} \cdot \overline{\overline{Q}}_e}{2}\right) - \sqrt{\frac{\epsilon_0}{\mu_0}}\hat{\mathbf{r}} \times \mathbf{p}_m\right], \quad (9)$$

$$\mathbf{H}(\mathbf{r}) - \mathbf{H}^{inc}(\mathbf{r}) \approx k^2 \frac{e^{-jkr}}{4\pi\mu_0 r}\left[(\mathbf{I} - \hat{\mathbf{r}}\hat{\mathbf{r}}) \cdot \left(\mathbf{p}_m + jk\frac{\hat{\mathbf{r}} \cdot \overline{\overline{Q}}_m}{2}\right) + \sqrt{\frac{\mu_0}{\epsilon_0}}\hat{\mathbf{r}} \times \mathbf{p}_e\right], \quad (10)$$

where

$$\mathbf{p}_e = \int_V (\epsilon - \epsilon_0)\mathbf{E}(\mathbf{r})dV(\mathbf{r}) \quad \text{and} \quad \mathbf{p}_m = \int_V (\mu - \mu_0)\mathbf{H}(\mathbf{r})dV(\mathbf{r}), \quad (11)$$

are the electric and magnetic dipole moments of the scatterer, respectively, see [10, 11] and [12, Sect. 7.10]. In terms of the electric and magnetic polarisation currents, defined in (2) and (1), they are

$$\mathbf{p}_e = \frac{1}{j\omega}\int_V \mathbf{J}_e(\mathbf{r})dV(\mathbf{r}), \quad \text{and} \quad \mathbf{p}_m = \frac{1}{j\omega}\int_V \mathbf{J}_m(\mathbf{r})dV(\mathbf{r}). \quad (12)$$

However, also an electric current distribution may exhibit a magnetic dipole moment when defined through [12, Sect. 7.10]

$$\mathbf{p}_m = \frac{\mu_0}{2}\int_V \mathbf{r} \times \mathbf{J}_e(\mathbf{r})dV(\mathbf{r}). \quad (13)$$

This is a non-static term, proportional to the frequency ω. As a dual to the former, the magnetic current similarly induces an electric dipole moment defined by

$$\mathbf{p}_e = -\frac{\epsilon_0}{2}\int_V \mathbf{r} \times \mathbf{J}_m(\mathbf{r})dV(\mathbf{r}). \quad (14)$$

Finally,

$$\overline{\overline{Q}}_e = \int_V \frac{\mathbf{r}\mathbf{J}_e(\mathbf{r}) + \mathbf{J}_e(\mathbf{r})\mathbf{r}}{j\omega}dV(\mathbf{r}), \quad \text{and} \quad (15)$$

$$\overline{\overline{Q}}_m = \int_V \frac{\mathbf{r}\mathbf{J}_m(\mathbf{r}) + \mathbf{J}_m(\mathbf{r})\mathbf{r}}{j\omega}dV(\mathbf{r}) \quad (16)$$

define the electric and magnetic quadrupole dyadics [12], respectively.

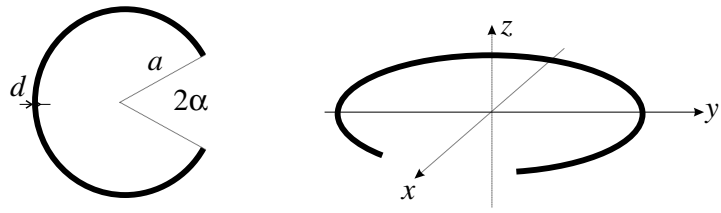

Figure 1. Geometry of the split-ring element.

3. SCATTERING OF A CIRCULAR WIRE RING

Let us now consider a circular ring of radius a in the xy-plane and centred at the origin (Figure 1). The ring consists of a thin perfectly conducting wire of diameter d and a gap of total angle 2α. The ring is irradiated by an electromagnetic field with components $E^{inc}_{x,0}$, $E^{inc}_{y,0}$, $E^{inc}_{z,0}$ of the electric and $H^{inc}_{x,0}$, $H^{inc}_{y,0}$, $H^{inc}_{z,0}$ of the magnetic field. Henceforth, the sub-index '0' is omitted, since we are dealing primarily with the quasi-static field quantities.

The problem is next divided into two independent sub-problems: one for the excitation through the electric field and one for the magnetic field, and the effect of a narrow gap located in the interval $\varphi \in [-\alpha, \alpha]$ is analysed separately for each possible excitation and polarisation. Besides the purely electric and purely magnetic polarisation, there is also cross-coupling from magnetic induction to electric polarisation and vice versa, from electric field to magnetic polarisation. In a reciprocal medium the cross coupling should be the same both ways.

3.1. Electric Field Excitation

3.1.1. Field Parallel to the Ring

Let us first consider the case of an electric field acting in the plane of the ring, such that $\mathbf{E}^{inc} = E^{inc}_x \hat{\mathbf{x}} + E^{inc}_y \hat{\mathbf{y}}$. The corresponding potential being then $\Phi^{inc} = -xE^{inc}_x - yE^{inc}_y$, our task is to determine the distribution of charges arising on the wire such that the total potential

$$\Phi^{inc} + \Phi^{sc} = \text{constant} \tag{17}$$

on the surface of the ring. Setting the constant = 0, the scattered potential is

$$\Phi^{sc} = \left(\cos\varphi E_x^{inc} + \sin\varphi E_y^{inc}\right) \cdot \begin{cases} \left(a+\frac{d}{2}\right) & \text{on the outer rim,} \\ \left(a-\frac{d}{2}\right) & \text{on the inner rim,} \\ a & \text{on the upper and lower rim.} \end{cases} \quad (18)$$

In the thin wire approximation (when $d \ll a$), Φ^{sc} may be seen as a result of a line charge $\varrho_e(\varphi)$ distributed along the centre-line of the wire at $\boldsymbol{\rho} = a\hat{\boldsymbol{\rho}}$ and complemented by a radial line dipole $\mathbf{P}_e^{\rho} = \hat{\boldsymbol{\rho}} P_e^{\rho}(\varphi)$ canceling the remaining potential difference between the inner and outer rim. The integral Equation (7) can then be expressed in terms of the unknown line charge and radial dipole density distributions as

$$\Phi^{sc} = \frac{1}{4\pi\epsilon_0}\int_0^{2\pi} \frac{\varrho_e(\varphi')ad\varphi'}{\sqrt{|\rho-\rho'|^2+z^2}} + \frac{1}{4\pi\epsilon_0}\int_0^{2\pi} P_e^{\rho}(\varphi')\frac{\partial}{\partial\rho'}\frac{ad\varphi'}{\sqrt{|\rho-\rho'|^2+z^2}}. \quad (19)$$

Along the upper or lower rim

$$\begin{aligned} &\Phi^{sc} \\ &= \frac{1}{4\pi\epsilon_0}\int_0^{2\pi} \frac{\varrho_e(\varphi')ad\varphi'}{\sqrt{(a\cos\varphi - a\cos\varphi')^2 + (a\sin\varphi - a\sin\varphi')^2 + \left(\frac{d}{2}\right)^2}} \\ &= \frac{1}{4\pi\epsilon_0}\int_0^{2\pi} \frac{\varrho_e(\varphi')ad\varphi'}{\sqrt{2a^2 - 2a^2\cos(\varphi-\varphi') + (\frac{d}{2})^2}} \\ &\approx \frac{1}{8\pi\epsilon_0}\int_0^{2\pi} \frac{\varrho_e(\varphi')d\varphi'}{|\sin\left(\frac{\varphi-\varphi'}{2}\right)|}, \end{aligned} \quad (20)$$

where the singularity of the last integral is to be evaluated in the principal value sense, by excluding the angle $\pm\frac{d}{2a}$ around the singularity at $\varphi' = \varphi$. The equation is satisfied by a charge distribution of the form $\varrho_e = A_y\sin\varphi + A_x\cos\varphi$, which yields

$$\Phi^{sc} = a\left(\cos\varphi E_x^{inc} + \sin\varphi E_y^{nc}\right) \approx (A_x\cos\varphi + A_y\sin\varphi)\frac{\ln\left(\frac{8a}{d}\right)-2}{2\pi\epsilon_0}. \quad (21)$$

Noting that $\ln(8a/d) - 2 \approx \ln(a/d)$ when $a \gg d$, the relevant coefficients can be written

$$A_x \approx \frac{2\pi\epsilon_0 a E_x^{inc}}{\ln\left(\frac{a}{d}\right)}, \quad A_y \approx \frac{2\pi\epsilon_0 a E_y^{inc}}{\ln\left(\frac{a}{d}\right)}. \quad (22)$$

The charge ϱ_e can be equivalently written in terms of a distribution of line dipoles along the wire satisfying $\nabla \cdot \mathbf{P}_e^{\varphi} = -\varrho_e$ with the density

$$\mathbf{P}_e^{\varphi}(\rho) = \hat{\boldsymbol{\varphi}} a (A_y \cos\varphi - A_x \sin\varphi). \tag{23}$$

The second part of the scattered potential (19) arises from the transversal (i.e., radially directed) line dipole distribution $\mathbf{P}_e^{\rho}(\varphi)$ governed by

$$\begin{aligned} &\frac{d}{2}(\cos\varphi E_x^{inc} + \sin\varphi E_y^{inc}) \\ &= \frac{-1}{\pi\epsilon_0}\int_0^{2\pi} \frac{P_e^{\rho}(\varphi')(a - \rho\cos(\varphi-\varphi'))ad\varphi'}{(a^2+\rho^2-2a\rho\cos(\varphi-\varphi'))^{3/2}} \\ &\approx \frac{-1}{16\pi\epsilon_0}\int_0^{2\pi} \frac{P_e^{\rho}(\varphi')d\varphi'}{a\left|\sin\left(\frac{\varphi-\varphi'}{2}\right)\right|}. \end{aligned} \tag{24}$$

The Ansatz $P_e^{\rho}(\varphi) = a(A'_x \cos\varphi + A'_y \sin\varphi)$ gives again the principal value

$$\frac{d}{2}\left(\cos\varphi E_x^{inc} + \sin\varphi E_y^{inc}\right) \approx -\left(A'_x\cos\varphi + A'_y\sin\varphi\right)\frac{\ln\left(\frac{8a}{d}\right)-2}{4\pi\epsilon_0}. \tag{25}$$

Hence, the two desired coefficients are

$$A'_x \approx -\frac{2\pi d\epsilon_0 E_x^{inc}}{\ln\left(\frac{a}{d}\right)}, \quad A'_y \approx -\frac{2\pi d\epsilon_0 E_y^{inc}}{\ln\left(\frac{a}{d}\right)}. \tag{26}$$

Integration of the two dipole density distributions gives the total dipole moment:

$$\mathbf{p}_e = \int_0^{2\pi} (\mathbf{P}_e^{\varphi} + \mathbf{P}_e^{\rho}) a d\varphi \approx \frac{2\pi^2\epsilon_0 a^2}{\ln\left(\frac{a}{d}\right)}(a-d)\left(E_x^{inc}\hat{\mathbf{x}} + E_y^{inc}\hat{\mathbf{y}}\right). \tag{27}$$

The introduction of a gap of angular width 2α at $\varphi \in [-\alpha, \alpha]$ entails a change in the circumferential or φ-directed dipole distributions, while the transversal or ρ-directed dipole density distributions remain in the main unaffected. In particular, for a y-polarised electric field there arises, in addition to the charge induced on the unbroken ring, an additional uniform distribution of dipoles along the wire such that the total line dipole density obeys

$$\mathbf{P}_e^{\varphi}(\varphi) = aA_y\left(\cos\varphi - (1-\delta_\alpha)\right)\hat{\boldsymbol{\varphi}}, \tag{28}$$

where $\delta_\alpha = 1$ when the gap is closed ($\alpha = 0$) and zero otherwise (δ_α is the Kronecker symbol). However, for a y-directed field, opposite charges will also accumulate on the tips of the wire, so that the gap forms a y-directed dipole with a dipole moment $\mathbf{p}_e = \pi\alpha\epsilon_0 a d^2 E_y^{inc}/2\hat{\mathbf{y}}$.

When the electric field is x-polarised, the $\cos\varphi$-distribution must be modified in order to meet the condition of zero net charge on the ring. In fact, the function $\varrho_e(\varphi) = -A_x \cos\pi\frac{\varphi-\pi}{\pi-\alpha}$, which for α being small is $\approx A_x(\cos\varphi - \alpha(1-\frac{\varphi}{\pi})\sin\varphi + \ldots)$, can be seen to respect the requirement of a vanishing net charge and also smoothly approach the exact distribution of the unbroken ring ($\alpha = 0$). Thus, the corresponding dipole distribution is

$$\mathbf{P}_e^{\varphi}(\varphi) = aA_x(1-\alpha/\pi)\sin\left(\pi\frac{\varphi-\pi}{\pi-\alpha}\right)\hat{\boldsymbol{\varphi}}. \tag{29}$$

Integrating $\mathbf{P}_e^{\varphi}$ and $\mathbf{P}_e^{\rho}$ over the split-ring for both x and y-polarisation, the total dipole moment is found to be

$$\begin{aligned}&\mathbf{p}_{e,tot}\\ &= a^2\hat{\mathbf{y}}\left[A_y(\pi-\alpha+(2\delta_\alpha-\cos\alpha)\sin\alpha) + A'_y(\pi-\alpha+\frac{\sin 2\alpha}{2})\right]\\ &\quad + a^2\hat{\mathbf{x}}\left[2A_x\frac{(\pi-\alpha)^2}{(2\pi-\alpha)\alpha}\sin\alpha + A'_x(\pi-\alpha-\frac{\sin 2\alpha}{2})\right]\end{aligned} \tag{30}$$

Requiring that $\alpha \ll 1$, the first order approximation is

$$\mathbf{p}_{e,tot} \approx \frac{2\pi^2\epsilon_0 a^2}{\ln\left(\frac{a}{d}\right)}\left[E_y^{inc}\hat{\mathbf{y}}(a-d) + E_x^{inc}\hat{\mathbf{x}}\left(a-d-\frac{\alpha}{\pi}\left(\frac{3}{2}a-2d\right)\right)\right]. \tag{31}$$

Thus, the gap changes the dipole moment in the x-direction more sensibly than in the y-direction. The distributions (28) and (29) are seen to agree with electromagnetic NEC-simulations of the currents on a very thin split-ring of 1 cm radius at 333 MHz and 1 GHz, see Figure 2.

Now we turn to the higher-order multipole moments. On account (13), the magnetic dipole in the direction of the ring's axis is given by

$$\begin{aligned}\mathbf{p}_m &= \frac{j\omega\mu_0}{2}\int_{\alpha}^{2\pi-\alpha}\rho\times(\mathbf{P}_e^{\varphi}+\mathbf{P}_e^{\rho})ad\varphi\\ &= -j\omega\mu_0 a^3 A_y((\pi-\alpha)(1-\delta_\alpha)+\sin\alpha))\hat{\mathbf{z}}\\ &\approx -j2\pi^2(1-\delta_\alpha)\omega\mu_0\epsilon_0 a^4\frac{E_y^{inc}}{\ln\left(\frac{a}{d}\right)}\hat{\mathbf{z}},\end{aligned} \tag{32}$$

where the last approximation holds for $\alpha \ll 1$. However, when $\alpha = 0$, the magnetic dipole totally vanishes. Thus, there is a real discontinuity involved: the magnetic dipole vanishes as soon as the gap is closed since the gap cuts the flow of current through that branch of the ring.

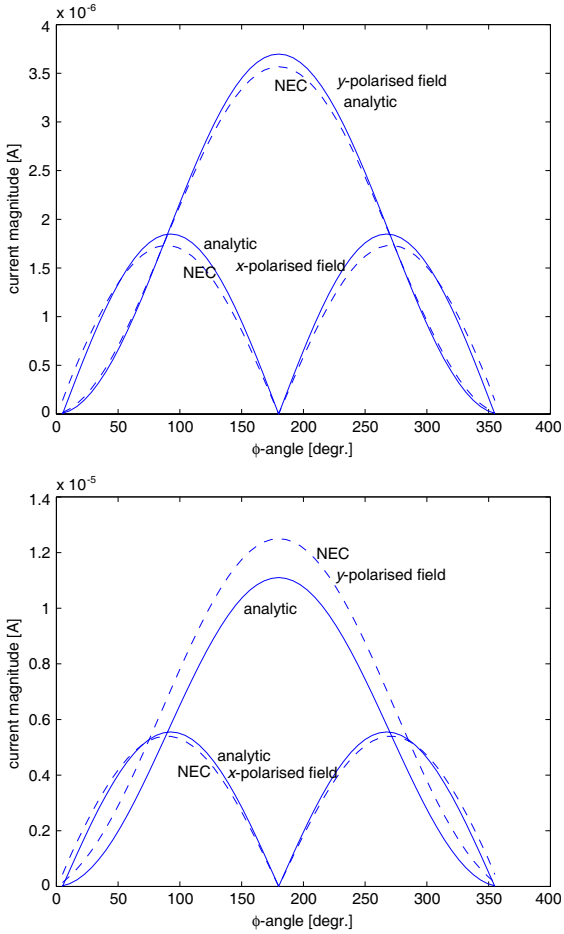

Figure 2. Results of NEC simulations of the current density along the wire for the two orthogonal polarisations in the plane of the ring. The dimensions of the ring are $a = 1\,\mathrm{cm}$, $d = 0.02\,\mathrm{mm}$, and $2\alpha = 10^\circ$. Top figure is for $f = 333\,\mathrm{MHz}$, bottom for $f = 1\,\mathrm{GHz}$. It is seen that the analytical model is more accurate for the lower frequency.

Additionally, the dipole in the gap creates a magnetic dipole of moment $\mathbf{p}_m \approx j\omega\mu_0\epsilon_0\pi\alpha a d^2 E_y^{inc}/4\hat{\mathbf{z}}$. From (16) the dominant contribution of the quadrupole moment is

$$\overline{\overline{Q}}_e \approx \frac{8\pi\alpha\epsilon_0 a^4 E_x^{inc}}{3\ln\left(\frac{a}{d}\right)}\left[\hat{\mathbf{y}}\hat{\mathbf{y}} - \left(1 - \frac{3d}{2a}\right)\hat{\mathbf{x}}\hat{\mathbf{x}}\right] \tag{33}$$

when only the first-order terms for $\alpha \ll 1$ are retained. Thus, the

quadrupole moment vanishes when the gap closes up, $\alpha \to 0$, as expected.

3.1.2. Field Perpendicular to the Ring

When the electric field acts perpendicularly to the plane of the ring, the potential is $\Phi^{inc} = -\frac{d}{2}E_z^{inc}$ on the upper and $\Phi^{inc} = \frac{d}{2}E_z^{inc}$ on the lower rim of the ring. In order to satisfy the boundary condition (17), a z-directed line dipole $\mathbf{P}_e^z(\varphi) = \hat{\mathbf{z}}P_e^z(\varphi)$ must be introduced, which is distributed along the centre-line of the ring. Its scalar potential is

$$\begin{aligned}\Phi^{sc} &= \frac{-1}{4\pi\epsilon_0}\frac{\partial}{\partial z}\int_0^{2\pi}\frac{P_e^z(\varphi')ad\varphi'}{\sqrt{|\rho-\rho'|^2+z^2}} \\ &= \frac{1}{4\pi\epsilon_0}\int_0^{2\pi}\frac{P_e^z(\varphi')zad\varphi'}{(a^2+\rho^2+z^2-2a\rho\cos(\varphi-\varphi'))^{3/2}},\end{aligned} \tag{34}$$

and in particular along the upper rim ($z = \frac{d}{2}$)

$$\Phi^{sc} \approx \frac{d}{64\pi\epsilon_0 a^2}\int_0^{2\pi}\frac{P_e^z(\varphi')d\varphi'}{|\sin\left(\frac{\varphi-\varphi'}{2}\right)|^3}. \tag{35}$$

and the same but negative on the lower rim, $z = -\frac{d}{2}$. Evaluating the integral in the principal value sense with $P_e^z(\varphi) = A_z a$ as a trial function yields

$$\frac{d}{2}E_z^{inc} \approx \frac{A_z d}{2\pi\epsilon_0 a(d/2a)^2}. \tag{36}$$

Thus we find $A_z = \pi\epsilon_o d^2 E_z^{inc}/4a$, and hence the total electric dipole moment in the z-direction becomes

$$\mathbf{p}_e \approx 2(\pi-\alpha)a^2 A_z\hat{\mathbf{z}} = \frac{\pi}{2}(\pi-\alpha)\epsilon_0 a d^2 E_z^{inc}\hat{\mathbf{z}}, \tag{37}$$

when the gap at $\varphi \in [-\alpha, \alpha]$ is taken into account. Additionally, there arises a magnetic dipole and an electric quadrupole with the respective moments

$$\begin{aligned}\mathbf{p}_m &= \frac{j\omega\mu_0}{2}\int_\alpha^{2\pi-\alpha}\boldsymbol{\rho}\times\hat{\mathbf{z}}a^2A_z d\varphi = j\omega\mu_0 a^3 A_z\sin\alpha\hat{\mathbf{y}} \\ &\approx j\frac{\pi}{4}\alpha\omega\mu_0\epsilon_o a^2 d^2 E_z^{inc}\hat{\mathbf{y}},\end{aligned} \tag{38}$$

$$\overline{\overline{Q}}_e = \int_\alpha^{2\pi-\alpha}(\boldsymbol{\rho}\hat{\mathbf{z}}+\hat{\mathbf{z}}\boldsymbol{\rho})A_z a^3 d\varphi \approx -\frac{\pi}{2}\alpha\epsilon_0 d^2 a^2 E_z^{inc}(\hat{\mathbf{x}}\hat{\mathbf{z}}+\hat{\mathbf{z}}\hat{\mathbf{x}}), \tag{39}$$

both of which are seen to vanish when the gap closes up, $\alpha \to 0$.

3.2. Magnetic Field Excitation

In the magnetostatic problem, the magnetic dipole moment of the ring is determined from the condition of zero magnetic induction *through the wire*, such that the magnetic field component normal to the surface vanishes on the ring (i.e., $\hat{\mathbf{n}}\cdot(\mathbf{H}^{inc}+\mathbf{H}^{sc})=0$, where $\hat{\mathbf{n}}(\mathbf{r})$ is the surface normal at $\mathbf{r}$).

3.2.1. Field Parallel to the Ring

We begin by considering the case of an incident magnetic field acting in the plane of the ring. Then, along the outer rim of the ring $\hat{\mathbf{n}}\cdot\mathbf{H}^{inc}=\cos\varphi H_x^{inc}+\sin\varphi H_y^{inc}$ and, correspondingly, along the inner rim $\hat{\mathbf{n}}\cdot\mathbf{H}^{inc}=-\cos\varphi H_x^{inc}-\sin\varphi H_y^{inc}$. To satisfy the boundary condition, a radially directed magnetic line dipole distribution $\mathbf{P}_m^{\rho}(\varphi)=\hat{\boldsymbol{\rho}}P_m^{\rho}(\varphi)$ is introduced along the centre-line of the wire, giving rise to the magnetic scalar potential

$$\Psi^{sc}=\frac{-1}{4\pi\mu_0}\int_0^{2\pi}\frac{P_m^{\rho}(\varphi')(a-\rho\cos(\varphi-\varphi'))ad\varphi'}{(a^2+\rho^2-2a\rho\cos(\varphi-\varphi'))^{3/2}}, \tag{40}$$

in the xy-plane ($z=0$). The normal (ρ) component of the magnetic field along the outer rim is thus

$$\hat{\boldsymbol{\rho}}\cdot\mathbf{H}^{sc}=-\hat{\boldsymbol{\rho}}\cdot\nabla\Psi^{sc}\approx\frac{1}{64\pi\mu_0}\int_0^{2\pi}\frac{P_m^{\rho}(\varphi')(\cos(\varphi-\varphi')-3)d\varphi'}{a^2|\sin(\frac{\varphi-\varphi'}{2})|^3}. \tag{41}$$

A suitable Ansatz is $P_m^{\rho}(\varphi)=a(C_x\cos\varphi+C_y\sin\varphi)$, where C_x and C_y are constants. By evaluating the singularity in the principal value sense we get

$$-\left(\cos\varphi H_x^{inc}+\sin\varphi H_y^{inc}\right)\approx\frac{C_x\cos\varphi+C_y\sin\varphi}{\pi\mu_0 a(d/2a)^2}, \tag{42}$$

with $C_x=-\pi\mu_0 d^2H_x^{inc}/4a$ and $C_y=-\pi\mu_0 d^2H_y^{inc}/4a$ following an application of the boundary condition. Thus, taking the gap into account, the total magnetic dipole moment is

$$\begin{aligned}\mathbf{p}_m&=\int_{\alpha}^{2\pi-\alpha}\mathbf{P}_m^{\rho}(\varphi')ad\varphi'=a^2\left(\pi-\alpha+\frac{\sin 2\alpha}{2}\right)(C_x\hat{\mathbf{x}}+C_y\hat{\mathbf{y}})\\&\approx-\frac{\pi^2}{4}\mu_0 ad^2\left(H_x^{inc}\hat{\mathbf{x}}+H_y^{inc}\hat{\mathbf{y}}\right).\end{aligned} \tag{43}$$

Furthermore, a magnetic dipole is built up across the gap because of the magnetic charges that prevent the magnetic flux to enter into the

wire. The magnetic charges at the end-surfaces are $\pm\pi(d/2)^2\mu_0 H_y^{inc}$ and their mutual distance is $2a\alpha$. Thus the magnetic dipole moment is $\mathbf{p}_m = -\pi\alpha\mu_0 a d^2 H_y^{inc}/2\hat{\mathbf{y}}$.

The principal higher order multipoles include in this case the electric dipole and the magnetic quadrupole. The ρ-directed magnetic polarisation contributes nothing since from (14) it follows that

$$\mathbf{p}_e = -\frac{j\omega\epsilon_0 a}{2}\int_{\alpha}^{2\pi-\alpha} \hat{\boldsymbol{\rho}}\times\hat{\boldsymbol{\rho}}(C_x\cos\varphi + C_y\sin\varphi)ad\varphi = 0, \qquad (44)$$

while the magnetic dipole in the gap produces the electric dipole moment $\mathbf{p}_e = -j\omega\epsilon_0\mu_0\pi\alpha a^2 d^2 H_y^{inc}/4\hat{\mathbf{z}}$.

The magnetic quadrupole moment of the wire is

$$\overline{\overline{Q}}_m = \int_{\alpha}^{2\pi-\alpha} [\boldsymbol{\rho}\mathbf{P}_m^{\rho} + \mathbf{P}_m^{\rho}\boldsymbol{\rho}]\, ad\varphi \approx -4a^3 C_x\alpha\hat{\mathbf{x}}\hat{\mathbf{x}} = \pi\alpha\mu_0 a^2 d^2 H^{inc}\hat{\mathbf{x}}\hat{\mathbf{x}}, \quad (45)$$

when α is small. The quadrupole moment contributed by the magnetic dipole formed by the gap is $\overline{\overline{Q}}_m \approx -\pi\alpha\mu_0 a^2 d^2 H_y^{inc}/2(\hat{\mathbf{y}}\hat{\mathbf{x}} + \hat{\mathbf{x}}\hat{\mathbf{y}})$.

3.2.2. Field Perpendicular to the Ring

Next, the incident magnetic field is assumed to be z-directed, so that $\hat{\mathbf{n}}\cdot\mathbf{H}^{inc} = \pm H_z^{inc}$ along the upper rim (+ sign) and the lower rim of the wire (− sign), respectively. To satisfy the boundary condition, a z-directed magnetic line dipole $\mathbf{P}_m^z(\varphi) = \hat{\mathbf{z}}P_m^{dip}(\varphi)$ is introduced along the centre-line. It gives rise to a magnetic scalar potential

$$\begin{aligned}\Psi^{sc} &= \frac{-1}{4\pi\mu_0}\frac{\partial}{\partial z}\int_0^{2\pi}\frac{P_m^z(\varphi')ad\varphi'}{\sqrt{|\rho-\rho'|^2+z^2}} \\ &= \frac{1}{4\pi\mu_0}\int_0^{2\pi}\frac{P_m^z(\varphi')zad\varphi'}{\left(a^2+\rho^2+z^2-2a\rho\cos(\varphi-\varphi')\right)^{3/2}}, \end{aligned} \qquad (46)$$

and hence the z-component of the magnetic field along the upper rim ($z = \frac{d}{2}$) will be

$$\hat{\mathbf{z}}\cdot\mathbf{H}^{sc} = -\hat{\mathbf{z}}\cdot\nabla\Psi^{sc} \approx \frac{-1}{32\pi\mu_0}\int_0^{2\pi}\frac{P_m^z(\varphi')d\varphi'}{a^2\left|\sin\left(\frac{\varphi-\varphi'}{2}\right)\right|^3}. \qquad (47)$$

A suitable magnetisation function is $P_m^z(\varphi) = aC_z$ (a constant), because the result is a uniform field

$$H_z^{inc} \approx \frac{-C_z}{\pi\mu_0 a(d/2a)^2}, \qquad (48)$$

which renders the coefficient $C_z = -\pi\mu_0 d^2 H_z^{inc}/4a$. Thus, the total magnetic dipole moment of the ring with a gap will be

$$\mathbf{p}_m \approx 2(\pi-\alpha)a^2 C_z \hat{\mathbf{z}} = -\frac{(\pi-\alpha)}{2}\pi\mu_0 a d^2 H_z^{inc}\hat{\mathbf{z}}. \tag{49}$$

The electric dipole and the magnetic quadrupole arising from the magnetisation are, respectively,

$$\begin{aligned}\mathbf{p}_e &= -\frac{j\omega\epsilon_0}{2}\int_{\alpha}^{2\pi-\alpha} \boldsymbol{\rho}\times\hat{\mathbf{z}}a^2 C_z d\varphi = -j\omega\epsilon_0 a^3 C_z \sin\alpha\hat{\mathbf{y}} \\ &\approx j\frac{\pi}{4}\alpha\omega\mu_0\epsilon_0 a^2 d^2 H_z^{inc}\hat{\mathbf{y}}, \end{aligned}\tag{50}$$

$$\begin{aligned}\overline{\overline{Q}}_m &= \int_{\alpha}^{2\pi-\alpha}(\boldsymbol{\rho}\hat{\mathbf{z}}+\hat{\mathbf{z}}\boldsymbol{\rho})C_z a^2 d\varphi = -2a^3 C_z\sin\alpha(\hat{\mathbf{x}}\hat{\mathbf{z}}+\hat{\mathbf{z}}\hat{\mathbf{x}}) \\ &\approx \frac{\pi}{2}\alpha\mu_0 a^2 d^2 H_z^{inc}(\hat{\mathbf{x}}\hat{\mathbf{z}}+\hat{\mathbf{z}}\hat{\mathbf{x}}). \end{aligned}\tag{51}$$

Faraday's induction law predicts an electrometric force to appear across the gap. The potential between the tips of the wire corresponds to a uniform electric field of intensity

$$\mathbf{E} = \frac{j\omega a\mu_0}{2}H_z^{inc}\hat{\boldsymbol{\varphi}}, \tag{52}$$

when the gap is assumed to be narrow. Thus, the wire is electrically polarised along its circumference $2\pi a$, and as the charge density on the wire is linear, the line dipole will obey the density function

$$\mathbf{P}(\varphi) = -p_e\frac{\varphi}{4}\left(2-\frac{\varphi}{\pi}\right)\hat{\boldsymbol{\varphi}}, \tag{53}$$

because its integral $\int_0^{2\pi}\mathbf{P}(\varphi)d\varphi = p_e\hat{\mathbf{y}}$, where p_e is the polarisability of the wire. The longitudinal dipole moment of the wire is given by $p_e \approx 4\pi^2 a^3\epsilon_0/\ln(a/d)E$, where E is the applied field $j\omega a\mu_0 H_z^{inc}/2$ according to (52).

4. APPLICATION TO EFFECTIVE MEDIUM THEORY

In this section, we apply the previous results for the multipole moments to compute the effective material properties of a structure consisting of a large number of split-rings, similarly aligned and ordered, as shown in Figure 3. In the effective medium theory, the material properties are derived from the polarisability of the individual inclusions. In particular, we assume here that all the split-rings are aligned such that all rings have the same axis and that the gap points in the same direction. Other configurations are of course realisable following the same procedure as given next.

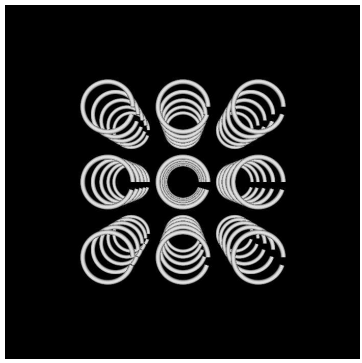

Figure 3. A 3D lattice of split-rings corresponding to the case $a = 10\,\text{mm}$ and $d = 2\,\text{mm}$. The size of a unit cell is $3a$ in every direction. Hence, the particle density is $N = 37000\,\text{m}^{-3}$.

4.1. Dipole Moments

Starting by taking only the dipole moments into account, we summarise the expressions for the dipole moments of a single split-ring in the previous section as

$$\begin{pmatrix} \mathbf{p}_e/\epsilon_0 \\ \mathbf{p}_m/\mu_0 \end{pmatrix} = \begin{pmatrix} \boldsymbol{\gamma}_{11} & \boldsymbol{\gamma}_{12} \\ \boldsymbol{\gamma}_{21} & \boldsymbol{\gamma}_{22} \end{pmatrix} \begin{pmatrix} \mathbf{E}^{inc} \\ \mathbf{H}^{inc} \end{pmatrix} = \boldsymbol{\gamma} \begin{pmatrix} \mathbf{E}^{inc} \\ \mathbf{H}^{inc} \end{pmatrix}. \tag{54}$$

Collecting the results, the explicit representation of the 6×6 polarisability matrix is (where $\eta_0 = \sqrt{\mu_0/\epsilon_0}$ is the wave impedance of vacuum, and $k = \omega\sqrt{\epsilon_0\mu_0}$ is the wave number in vacuum)

$$\boldsymbol{\gamma} = \begin{pmatrix} a_x & 0 & 0 & 0 & 0 & 0 \\ 0 & a_y & 0 & 0 & 0 & jkad_y\eta_0 \\ 0 & 0 & a_z & 0 & -jkad_z\eta_0 & 0 \\ 0 & 0 & 0 & b_x & 0 & 0 \\ 0 & 0 & jkac_y/\eta_0 & 0 & b_y & 0 \\ 0 & -jkac_z/\eta_0 & 0 & 0 & 0 & b_z \end{pmatrix} \tag{55}$$

with

$$a_x \approx 2\pi^2 a^2 \frac{(a-d)}{\ln(a/d)} \tag{56}$$

$$a_y \approx 2\pi^2 a^2 \frac{(a-d-\alpha(3a/2-2d)/\pi)}{\ln(a/d)} + \frac{\pi}{2}\alpha a d^2 \tag{57}$$

$$a_z \approx \frac{\pi}{2}(\pi-\alpha) a d^2 \tag{58}$$

$$b_x \approx -\frac{\pi^2}{4} a d^2 \tag{59}$$

$$b_y \approx -\frac{\pi^2}{4}\left(1+\frac{2\alpha}{\pi}\right)ad^2 \tag{60}$$

$$b_z \approx -\frac{\pi}{2}(\pi-\alpha)ad^2 \tag{61}$$

$$c_y = d_z \approx \frac{\pi}{4}\alpha ad^2 \tag{62}$$

$$c_z = d_y \approx \frac{2\pi^2 a^3}{\ln(a/d)} + \frac{\pi}{4}\alpha ad^2 \tag{63}$$

It is first of all seen that the $\boldsymbol{\gamma}$ matrix is hermitian symmetric, indicating a lossless particle. Also, every submatrix *viz.* the electric polarisability $\boldsymbol{\gamma}_{11}$, the cross terms $\boldsymbol{\gamma}_{12}$ and $\boldsymbol{\gamma}_{21}$, and the magnetic polarisability $\boldsymbol{\gamma}_{22}$ display anisotropy. The two preferred directions of the particle are the z-direction due to the plane of the split-ring, and the x-direction due to the direction of the gap.

Further we note that the (dominating part of the) (a_x, a_y) parameters scale as a^3, the (a_z, b_x, b_y, b_z) parameters scale as ad^2, $c_y = d_z$ scale as αad^2, and $c_z = d_y$ scale as a^3. Also, everywhere the angle α appears, it is multiplied by ad^2. We note an important difference between c_y and c_z: the former approaches zero as $\alpha \to 0$, whereas the latter does not. This is due to the fact that even if $\alpha \to 0$, our model assumes there is no galvanic connection across the gap. All off-diagonal terms are multiplied by the dimensionless factor ka, which is small ($\ll 1$) in the quasi-static limit.

In a dilute mixture, where the interaction between the particles can be neglected, the polarisation $\mathbf{P}$ and magnetisation $\mathbf{M}$ are given by

$$\begin{pmatrix} \mathbf{P}/\epsilon_0 \\ \mathbf{M} \end{pmatrix} = N\boldsymbol{\gamma}\begin{pmatrix} \mathbf{E}^{inc} \\ \mathbf{H}^{inc} \end{pmatrix}, \tag{64}$$

where N is the number density of the particles, i.e., the number of particles per unit volume. This defines the susceptibility $\boldsymbol{\chi} = N\boldsymbol{\gamma}$ of the material in the limit when $N\boldsymbol{\gamma} \to 0$.

When the particles are more densely packed, there is more interaction between them. In the low-frequency limit, where the average distance $R = N^{-1/3}$ between particles is much less than a wavelength, the interaction may be estimated by calculating the local field acting on one particle using the classical Lorentz field [13]

$$\begin{pmatrix} \mathbf{E}^{loc} \\ \mathbf{H}^{loc} \end{pmatrix} = \begin{pmatrix} \mathbf{E}^{inc} \\ \mathbf{H}^{inc} \end{pmatrix} + \frac{1}{3}\begin{pmatrix} \mathbf{P}/\epsilon_0 \\ \mathbf{M} \end{pmatrix}, \tag{65}$$

When the particle distance is comparable to wavelength, $kR > 1$, the local field must be calculated using the contributions from all

surrounding particles via the full Green's function as in [14]. In an infinite medium, the effect of this procedure is to replace the Lorentz factor 1/3 in the above equation by an interaction constant $C(\omega, \mathbf{k})$ [15, 16], depending on frequency ω and Bloch wavevector $\mathbf{k}$. In the static limit with a simple cubic lattice, the equation above is obtained. Considering $\mathbf{E}^{loc}$ and $\mathbf{H}^{loc}$ as the fields acting on each particle, the polarisation and the magnetisation are given by

$$\begin{pmatrix} \mathbf{P}/\epsilon_0 \\ \mathbf{M} \end{pmatrix} = N\boldsymbol{\gamma} \begin{pmatrix} \mathbf{E}^{loc} \\ \mathbf{H}^{loc} \end{pmatrix} = \boldsymbol{\chi} \begin{pmatrix} \mathbf{E}^{inc} \\ \mathbf{H}^{inc} \end{pmatrix}, \tag{66}$$

which defines the susceptibility $\boldsymbol{\chi}$ of the medium in the low frequency limit $kR \to 0$, and does not require $N\boldsymbol{\gamma} \to 0$. In total, the Lorentz field approach leads to the classical Clausius-Mossotti/Lorentz-Lorenz relation [3, 13] for the effective susceptibility matrix $\boldsymbol{\chi}$

$$\boldsymbol{\chi} = N\boldsymbol{\gamma}(\mathbf{I} - N\boldsymbol{\gamma}/3)^{-1}. \tag{67}$$

Since the $\boldsymbol{\gamma}$ matrix is hermitian symmetric, so is $\boldsymbol{\chi}$, and hence the constitutive relation

$$\begin{pmatrix} \mathbf{D}/\epsilon_0 \\ \mathbf{B}/\mu_0 \end{pmatrix} = (\mathbf{I} + \boldsymbol{\chi}) \begin{pmatrix} \mathbf{E}^{inc} \\ \mathbf{H}^{inc} \end{pmatrix} \tag{68}$$

is also hermitian symmetric, consistent with a lossless material.

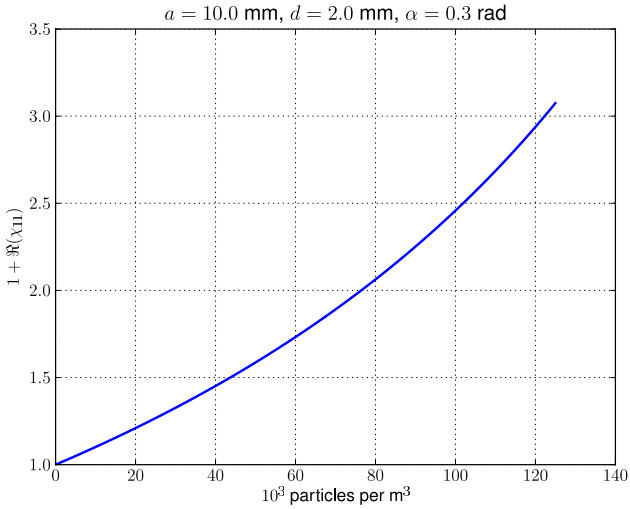

Figure 4. The behavior of the component $1 + \chi_{11}$, corresponding to the real part of ϵ_r in the x-direction, as a function of the particle density N.

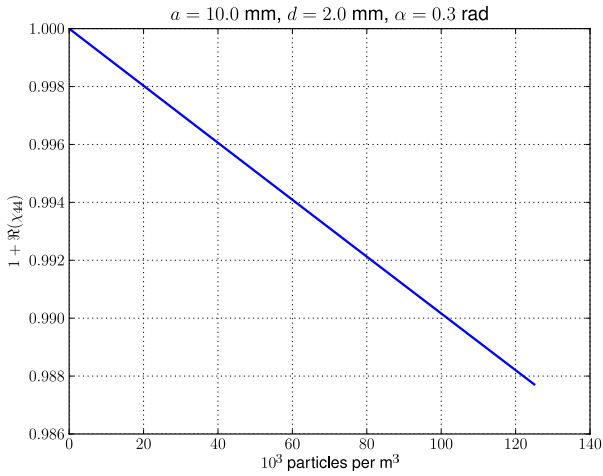

Figure 5. The behavior of the component $1 + \chi_{44}$, corresponding to the real part of μ_r in the x-direction, as a function of the particle density N.

Typical behavior of the (1, 1), (4, 4) and (2, 6)-components of $\mathbf{I} + \boldsymbol{\chi}$ is illustrated in Figures 4, 5 and 6, respectively, in the case that $a = 10\,\text{mm}$, $d = 2\,\text{mm}$, $k = 2\pi/0.1\,\text{m}^{-1}$ and $\alpha = 0.3$. Assuming the particles are packed in a simple cubic lattice, the highest possible number density is $N_{\max} = 1/(2a)^3 = 125000\,\text{m}^{-3}$. The trend of $\mu_r < 1$ seen in Figure 5 is consistent with the negative magnetic polarisability of perfectly conducting objects [11].

4.2. Non-existence of a Critical Density

From (67) it may be anticipated that the material is singular when $\det(\mathbf{I} - N\boldsymbol{\gamma}/3) = 0$. In this subsection, we show that this can only occur in a parameter region where the assumptions necessary for the homogenisation do not apply. These conditions require that the distances between the particles must be larger than the particles themselves and, at the same time, much smaller than a wavelength, in order for the Lorentz field to be applicable. For a cubic unit cell this condition can be formulated as $k^3 < N < 1/(2a)^3$.

The singular points occur when $\det(\mathbf{I} - N\boldsymbol{\gamma}/3) = 0$. The determinant can be shown to contain four factors, and hence the singularity conditions are

$$1 - a_x N/3 = 0,$$
$$1 - b_x N/3 = 0,$$

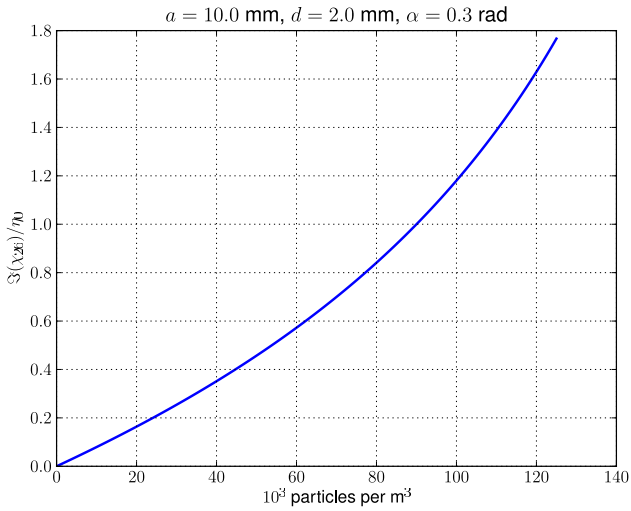

Figure 6. The behavior of cross-field component $\mathrm{Im}(\chi_{26}/\eta_0)$ as a function of the particle density N.

$$(1 - a_z N/3)(1 - b_y N/3) - (ka)^2 c_y d_z (N/3)^2 = 0, \quad \text{and}$$
$$(1 - a_y N/3)(1 - b_z N/3) - (ka)^2 c_z d_y (N/3)^2 = 0.$$

The first two conditions are independent of the frequency and violate the assumption $N < 1/(2a)^3$; thus, they do not apply. The third and the fourth conditions are less clear, and suggest two different resonant frequencies of the medium. The third condition corresponds to a frequency which is inversely proportional to the width of the gap and thus it escapes to infinity when the gap vanishes. The fourth condition needs further scrutiny. It can be written as

$$(ka)^2 c_z d_y = \left(\frac{3}{N}\right)^2 \left(1 - a_y \frac{N}{3}\right)\left(1 - b_z \frac{N}{3}\right), \tag{69}$$

whence

$$ka \approx \frac{\sqrt{\left(1 - \frac{N a_y}{3}\right)\left(1 - \frac{N b_z}{3}\right)}}{\frac{N\pi}{3}\left[\frac{2\pi a^3}{\ln(a/d)} + \frac{1}{4}\alpha a d^2\right]}, \tag{70}$$

where a_y and b_z are given by (57) and (61), respectively. This resonance corresponds to the transverse field components E_y and H_z, which is the combination of fields giving the strongest response of the medium, since the electric field is in the direction of the gap, and the magnetic field is normal to the split-ring plane.

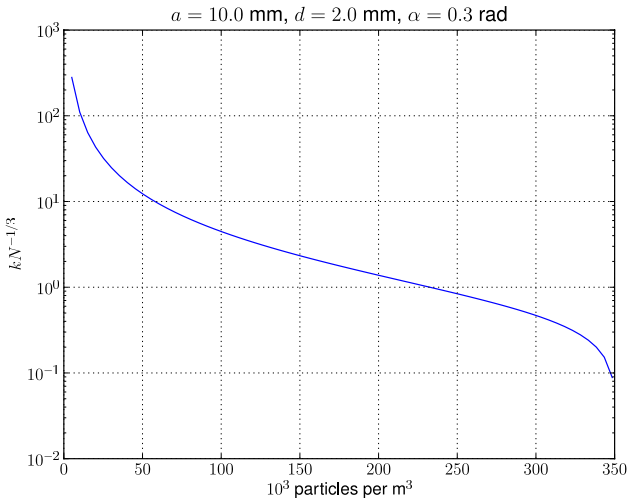

Figure 7. Illustration of (71). The number $kN^{-1/3}$ is the free space wave number k multiplied by the distance between adjacent split-rings, $N^{-1/3}$. For the quasi-static homogenisation to hold it must be smaller than unity, which requires $N > 240000\,\mathrm{m}^{-3}$.

The lower density limit of homogenisation is $kR < 1$, where $R = N^{-1/3}$ is the distance between adjacent particles. We can rewrite (70) in terms of kR as

$$kR \approx \frac{\frac{24}{\pi^2}\ln(a/d)}{(N(2a)^3)^{4/3}} \frac{\sqrt{\left(1-\frac{Na_y}{3}\right)\left(1-\frac{Nb_z}{3}\right)}}{1+\frac{\alpha}{4}\left(\frac{d}{a}\right)^2 \ln(a/d)} \tag{71}$$

from which it is seen that kR decreases if $N(2a)^3$ increases, but we must take the upper limit $N(2a)^3 < 1$ into account. In Figure 7, the quantity (71) is plotted as a function of N, using the dimensions of the rings given above. It is seen that $kR < 1$ requires $N > 240000\,\mathrm{m}^{-3}$, which violates the limit $N < 1/(2a)^3 = 125000\,\mathrm{m}^{-3}$. Thus, there can be no singularity of the material model in the parameter region where homogenisation is applicable.

It is possible to pack the rings tighter than in a simple cubic lattice, for instance by reducing the distance in the z direction, which could relax the condition $N < 1/(2a)^3$. However, this also implies corresponding changes in the Lorentz cavity field, which counteracts the effects of the gained density.

There is of course a very real resonance in the split-ring structure, but it is not captured by the quasi-static calculations in this paper. To include the resonance in a quasi-static setting, a more accurate modeling of the charge density close to the gap must be employed. One possibility is the slice generator used in [12] and [17], which in turn requires an *a priori* estimate of the resonance frequency.

4.3. Quadrupole Moments

The material model can be further refined by including information of the quadrupole moments of the particles. To start with, we note that in a quasi-static approximation, the field induced at a lattice point by surrounding identical quadrupole moments is zero due to symmetry. To include the effect of quadrupoles, the model needs to determine the electromagnetic response of the particle not only due to the field at its location, but also by the gradient of the field. This is a non-local material model, which can be used to increase the accuracy of the modeling of intermolecular interactions [18]. The quadrupole moments are expected to give a better understanding of the bulk properties of the material as has been shown for spherical inclusions [19–21], but the nonlocal nature of the model is troublesome in scattering problems, where the boundary has to be well defined. The present geometry is unfortunately not easily amenable for such consideration. Thus, we choose not to include the quadrupole moments in the material model at this level of understanding.

5. APPLICATIONS

Having derived the material properties of the split-ring medium in the quasi-static limit, we now interpret their meaning in terms of applications. The most straightforward application is considering the propagation of a plane wave. Denote the direction of propagation by the real unit vector $\hat{\mathbf{s}}$ and the refractive index by n, so that the fields are given by $\mathbf{E}(\mathbf{r}) = \mathbf{E}_0 e^{-jnk\hat{\mathbf{s}}\cdot\mathbf{r}}$ and $\mathbf{H}(\mathbf{r}) = \mathbf{H}_0 e^{-jnk\hat{\mathbf{s}}\cdot\mathbf{r}}$ with $\mathbf{E}_0$ and $\mathbf{H}_0$ being constant vectors. Inserting this Ansatz in Maxwell's equations and considering a dilute medium where $\boldsymbol{\chi} = N\boldsymbol{\gamma}$, we obtain

$$-jkn \begin{pmatrix} 0 & -\hat{\mathbf{s}}\times\mathbf{I} \\ \hat{\mathbf{s}}\times\mathbf{I} & 0 \end{pmatrix} \begin{pmatrix} \mathbf{E}_0 \\ \mathbf{H}_0 \end{pmatrix} = j\omega \begin{pmatrix} \epsilon_0\mathbf{I} & 0 \\ 0 & \mu_0\mathbf{I} \end{pmatrix} (\mathbf{I} + N\boldsymbol{\gamma}) \begin{pmatrix} \mathbf{E}_0 \\ \mathbf{H}_0 \end{pmatrix} \quad (72)$$

This is an eigenvalue problem with n (or $1/n$) as the eigenvalue, and $(\mathbf{E}_0, \mathbf{H}_0)$ as the eigenvector [22]. More explicitly, the existence of plane

waves requires the following determinant condition to hold:

$$\begin{vmatrix} 1+Na_x & 0 & 0 & 0 & -ns_z & ns_y \\ 0 & 1+Na_y & 0 & ns_z & 0 & -ns_x+jkaNc_z \\ 0 & 0 & 1+Na_z & -ns_y & ns_x-jkaNc_y & 0 \\ 0 & ns_z & -ns_y & 1+Nb_x & 0 & 0 \\ -ns_z & 0 & ns_x+jkaNc_y & 0 & 1+Nb_y & 0 \\ ns_y & -ns_x-jkaNc_z & 0 & 0 & 0 & 1+Nb_z \end{vmatrix} = 0 \tag{73}$$

From this equation the refractive index n can be calculated for each propagation direction $\hat{\mathbf{s}} = (s_x, s_y, s_z)$. For the three principal directions, the explicit solutions to the eigenvalue problem are easily

Table 1. Wave parameters and polarisations of plane waves propagating along the three principal directions in the effective medium. The wave impedances $\eta_{1,2}$ correspond to the ratio between the electric and magnetic field components orthogonal to the propagation direction. Note that only a scaling factor differs for $n_{1,2}$ for different principal propagation directions, whereas the frequency dependence is the same.

(s_x, s_y, s_z)	$(1,0,0)$	$(0,1,0)$	$(0,0,1)$
n_1	n_{1x}	$\sqrt{\frac{1+Nb_x}{1+Nb_y}}n_{1x}$	$\sqrt{\frac{1+Na_x}{1+Na_z}}n_{1x}$
η_1/η_0	$\frac{n_{1x}-jkaNc_y}{1+Na_z}$	$\frac{\sqrt{(1+Nb_y)(1+Nb_x)}}{n_{1x}}$	$\frac{n_{1x}}{\sqrt{(1+Na_z)(1+Na_x)}}$
pol	E_z, H_y	E_z, H_x, H_y	E_x, E_z, H_y
n_2	n_{2x}	$\sqrt{\frac{1+Na_x}{1+Na_y}}n_{2x}$	$\sqrt{\frac{1+Nb_x}{1+Nb_z}}n_{2x}$
η_2/η_0	$\frac{n_{2x}-jkaNc_z}{1+Na_y}$	$\frac{n_{2x}}{\sqrt{(1+Na_y)(1+Na_x)}}$	$\frac{\sqrt{(1+Nb_z)(1+Nb_x)}}{n_{2x}}$
pol	E_y, H_z	E_x, E_y, H_z	E_y, H_x, H_z

$$n_{1x} = \sqrt{(1+Na_z)(1+Nb_y)-(kaNc_y)^2}$$
$$n_{2x} = \sqrt{(1+Na_y)(1+Nb_z)-(kaNc_z)^2}$$

computed using Maple (http://www.maplesoft.com), and are given in Table 1. It is seen that for all principal directions the medium is birefringent with linearly polarised eigenwaves. The only TEM case is for propagation along the x-direction, for the other directions the waves are TE or TM. In addition, the first order frequency dependence due to the off-diagonal terms c_y and c_z is the same for all directions. All refractive indices decay with frequency in this low frequency limit. From (62) and (63) it is seen that $c_z \gg c_y$ if $a \gg d$, which means the frequency dependence of n_2 in Table 1 is stronger than that of n_1.

Another application of our results is related to [23, 24], where it is shown that the transmission through a low-pass slab of thickness d must satisfy (where the plane of incidence coincides with the xz-plane)

$$\int_0^\infty \ln \frac{1}{|T(\lambda)|} d\lambda \leq \frac{\pi^2 \gamma(\theta)}{2A\cos\theta}, \tag{74}$$

where

$$\gamma(\theta) = \begin{cases} \gamma_{exx}\cos^2\theta + \gamma_{ezz}\sin^2\theta + \gamma_{myy}, & \text{TM} \\ \gamma_{eyy} + \gamma_{mxx}\cos^2\theta + \gamma_{mzz}\sin^2\theta, & \text{TE.} \end{cases} \tag{75}$$

Here, $\gamma(\theta)/A$ is the static polarisability per unit area of a slab, with γ_e and γ_m being the electric and magnetic static polarisabilities, respectively. For a slab consisting of a dilute split-ring medium, assuming the z-direction in Figure 1 coincides with the normal direction of the slab with thickness t, we have

$$\frac{\gamma_{exx}}{At} = Na_x, \qquad \frac{\gamma_{eyy}}{At} = Na_y, \qquad \frac{\gamma_{ezz}}{At} = \frac{Na_z}{1+Na_z},$$
$$\frac{\gamma_{mxx}}{At} = Nb_x, \qquad \frac{\gamma_{myy}}{At} = Nb_y, \qquad \frac{\gamma_{mzz}}{At} = \frac{Nb_z}{1+Nb_z}.$$

Thus, the transmission blockage through a slab of the split-ring medium is restricted by

$$B\ln\frac{1}{T_0} \leq \frac{\pi^2 tN}{2\lambda_0\cos\theta} \begin{cases} a_x\cos^2\theta + \frac{a_z}{1+Na_z}\sin^2\theta + b_y, & \text{TM} \\ a_y + b_x\cos^2\theta + \frac{b_z}{1+Nb_z}\sin^2\theta, & \text{TE} \end{cases} \tag{76}$$

where T_0 is the maximum transmission level in the stop band (λ_1, λ_2), and $B = (\lambda_2 - \lambda_1)/\lambda_0$ is the relative bandwidth where $\lambda_0 = (\lambda_1 + \lambda_2)/2$ is the centre-wavelength. From the expressions for a_x etc and assuming $a \gg d$, we see that the polarisability is dominated by a_x and a_y, which are both proportional to a^3, whereas the other terms are proportional to ad^2. As comparison, a metal sphere with radius a has the electric polarisability $4\pi a^3$, which is larger than a_x if the wire thickness d is negligible. This is in agreement with the general result that the polarisability of any object is at most equal to the polarisability of

a circumscribed metallic object, which can be proven by variational methods [25, 26].

6. CONCLUSIONS

We have analysed the problem of scattering of electromagnetic waves from a small conducting wire ring furnished with a narrow gap. By solving integral equations, closed-form approximate expressions were derived for the electric and magnetic dipoles as well as the quadrupole moments of a single wire ring using assumptions of a low frequency (long wavelength) and a relatively thin wire with a narrow gap.

By homogenisation, or by linking these multipole moments to the macroscopic fields using the Clausius-Mossotti/Lorentz-Lorenz-approach, these expressions provide clear insight into how the electrical properties scale with the geometrical parameters. The constitutive equations of a bi-anisotropic medium consisting of an ordered assembly of aligned split-ring particles was written in terms of a 6×6 matrix containing ten nonzero components. The properties of the analytical material model were further studied and its limits of applicability were assessed. In particular, it was found that the possible resonance phenomenon, where the material parameters would experience a sudden change, occurs in a parameter region where the inclusion distances do not comply with the quasi-static assumptions, making the homogenisation approach not applicable. Thus, the model cannot dependably capture the material resonance.

Further, we gave two examples of how the material model may be used in applications. Expressions were given for the wave parameters in the principal propagation directions, and the polarisabilities were used together with the results from [23, 24] to give an upper bound on the product of bandwidth and transmission level for a slab of split-ring material used as a band-stop filter.

For future studies, inclusion of the quadrupole moments may be necessary, but their application is foreseen to be difficult. Nevertheless, the possibility is envisaged of developing medium models for particles endowed with a more complicated structure than the simple split-ring resonator.

REFERENCES

1. Engheta, N. and R. W. Ziolkowski (eds.), *Electromagnetic Metamaterials: Physics and Engineering Explorations*, Wiley, New York, 2006.

2. Pendry, J. B., A. J. Holden, D. J. Robbins, and W. J. Stewart, "Magnetism from conductors and enhanced nonlinear phenomena," *IEEE Microw. Theory and Techniques*, Vol. 47, 2075–2084, 1999.
3. Merlin, R., "Metamaterials and the Landau-Lifshitz permeability argument: Large permittivity begets high-frequency magnetism," *Proc. Nat. Acad. Sci.*, Vol. 106, No. 6, 1693–1698, Feb. 10, 2009.
4. Simovski, C. R. and B. Sauviac, "Toward creating isotropic microwave composites with negative refraction," *Radio Science*, Vol. 39, 1–18, 2004, RS2014.
5. Lewellyn Smith, S. G. and A. M. J. Davis, "The split ring resonator," *Proc. R. Soc. A*, Vol. 466, 3117–3134, 2010.
6. Movchan, A. B. and S. Guenneau, "Split-ring resonators and localized modes," *Phys. Rev. B*, Vol. 70, 125116, 2004.
7. Popa, B.-I. and S. A. Cummer, "Compact dielectric particles as a building block for low-loss magnetic metamaterials," *Phys. Rev. Lett.*, Vol. 1000, 207401, 2008.
8. Jones, D. S., "Low frequency electromagnetic radiation," *J. Inst. Maths Applics*, Vol. 23, 421–447, 1979.
9. Stevenson, A. F., "Solution of electromagnetic scattering problems as power series in the ratio (dimension of scatterer)/wavelength," *J. Appl. Phys.*, Vol. 24, 1134–1142, 1953.
10. Kleinman, R. E. and T. B. A. Senior, "Rayleigh scattering," V. K. Varadan and V. V. Varadan (eds.), *Low and High Frequency Asymptotics*, 1–70, North-Holland, 1986.
11. Arvas, E., R. F. Harrington, and J. R. Mautz, "Radiation and scattering from electrically small conducting bodies of arbitrary shape," *IEEE Trans. Antennas Propag.*, Vol. 34, No. 1, 66–77, Jan. 1986.
12. Van Bladel, J., *Electromagnetic Fields*, 2nd edition, IEEE Press & Wiley Interscience, 2007.
13. Jackson, J. D., *Classical Electrodynamics*, 3rd edition, Wiley, 1999.
14. Hadad, Y. and B. Z. Steinberg, "Electrodynamic synergy of micro-properties and macro-structure in particle arrays," *2010 URSI Electromagnetic Theory Symposium*, 839–842, 2010.
15. Belov, P. A. and C. R. Simovski, "On homogenization of electromagnetic crystals formed by uniaxial resonant scatterers," *Phys. Rev. E*, Vol. 72, 026615, 2005.
16. Silveirinha, M. G., "Generalized Lorentz-Lorenz formulas for microstructured materials," *Phys. Rev. B*, Vol. 76, 245117, 2007.

17. Bossavit, A., "Homogenization of split-ring arrays, seen as the exploitation of translational symmetry," *Metamaterials and Plasmonics: Fundamentals, Modelling, Applications*, 77–90, Springer Netherlands, 2008.
18. Holt, A. and G. Karlström, "Inclusion of the quadrupole moment when describing polarization. The effect of the dipole-quadrupole polarizability," *J. Comput. Chem.*, Vol. 29, 2033–2038, 2008.
19. Rayleigh, L., "On the influence of obstacles arranged in rectangular order upon the properties of the medium," *Phil. Mag.*, Vol. 34, 481–502, 1892.
20. McPhedran, R. C. and D. R. McKenzie, "The conductivity of lattices of spheres I. The simple cubic lattice," *Proc. R. Soc. Lond. A*, Vol. 359, 45–63, 1978.
21. Qi, J., H. Kettunen, H. Wallén, and A. Sihvola, "Quasi-dynamic homogenization of geometrically simple dielectric composites," *ACES Journal*, Vol. 25, No. 12, 1036–1045, 2010.
22. Sjöberg, D., "Simple wave solutions for the Maxwell equations in bianisotropic nonlinear media, with application to oblique incidence," *Wave Motion*, Vol. 32, No. 3, 217–232, 2000.
23. Gustafsson, M., C. Sohl, C. Larsson, and D. Sjöberg, "Physical bounds on the all-spectrum transmission through periodic arrays," *EPL Europhysics Letters*, Vol. 87, No. 3, 34002, 2009.
24. Sjöberg, D., M. Gustafsson, and C. Larsson, "Physical bounds on the all-spectrum transmission through periodic arrays: Oblique incidence," *EPL Europhysics Letters*, Vol. 92, 34009, 2010.
25. Sjöberg, D., "Variational principles for the static electric and magnetic polarizabilities of anisotropic media with perfect electric conductor inclusions," *J. Phys. A: Math. Theor.*, Vol. 42, 335403, 2009.
26. Jones, D. S., "Scattering by inhomogeneous dielectric particles," *Q. J. Mech. Appl. Math.*, Vol. 38, 135, 1985.